JOURNAL OF GUIDANCE, CONTROL, AND DYNAMICS
Vol. 31, No. 2, March–April 2008

Transition Flight Control of Two Vertical/Short Takeoff and Landing Aircraft

Yang Xili,* Fan Yong,† and Zhu Jihong‡
Tsinghua University, 100084 Beijing, People's Republic of China

DOI: 10.2514/1.29112

We propose two nonlinear approaches for the autonomous transition control of two vertical/short takeoff and landing aircraft. The first aircraft, referred to as the V-1 aircraft, is a fixed-wing fighter equipped with a vectored thrust and lift fan. The second aircraft is a tilt rotor. We provide nonlinear models for the transition from hover to forward flight. Both control problems are nonlinear, nonaffine, and have redundant inputs. Furthermore, some control inputs must reach specified end values when the transition has been completed. However, there is a key difference between the two aircraft. The V-1 aircraft can be controlled to rapidly increase velocity and pitch angle simultaneously, whereas the tilt rotor aircraft cannot, because linear and angular acceleration require conflicting control inputs from hover. For the V-1 aircraft, a method is applied whose key point is that a new controlled variable is appended to decrease the redundancy of the control inputs. For the tilt rotor aircraft, a second method is applied that transfers the problem into a two-time-scale problem. Nonlinear optimization is adopted to make the specified input approach the specified end value. We also consider problems associated with cases in which insufficient control power limits the ability of the aircraft to achieve commanded controlled variable rates. Simulations show that both approaches achieve the transition control successfully.

Nomenclature

$a_{x\mathrm{gc}}$ = component of the desired linear acceleration in the earth-fixed reference frame x axis
$a_{z\mathrm{gc}}$ = component of the desired linear acceleration in the earth-fixed reference frame z axis
C_D = drag coefficient
$\hat{C}_D$ = maximal magnitude of the uncertainty on the drag coefficient
C_L = lift coefficient
$\hat{C}_L$ = maximal magnitude of the uncertainty on the lift coefficient
C_m = pitching moment coefficient
$\hat{C}_m$ = maximal magnitude of the uncertainty on the pitching moment coefficient
$\bar{c}$ = mean aerodynamic chord
D_A = aerodynamic drag
F_{Txb} = component of thrust along the body x axis
F_{Tzb} = component of thrust along the body z axis
g = acceleration of gravity
H = height
I_{yy} = moment of inertia about the pitch axis
i, j = iteration index variables used in the optimization algorithm
L_A = aerodynamic lift
l_1 = distance from the root of the nacelle to the center of gravity (tilt rotor aircraft)
l_2 = distance from the root of the nacelle to tail (tilt rotor aircraft)
l_3 = distance from the root of the nacelle to hub (tilt rotor aircraft)
M = Mach number
M_T = moment generated by the engine
m = vehicle mass
m_A = aerodynamic pitching moment
n = nacelle angle (tilt rotor aircraft)
n_k = nacelle angle at step k (tilt rotor aircraft)
$n_{k+1}^{(i)}$ = nacelle angle of the number i iteration at step $k+1$ (tilt rotor aircraft)
$\dot{n}_{\max}$ = maximal nacelle angular velocity (tilt rotor aircraft)
q = pitching angular velocity
$\dot{q}_{ac}$ = desired pitching angular acceleration caused by aerodynamic effectors
$\dot{q}_c$ = desired pitching angular acceleration
$\dot{q}_{Tc}$ = desired pitching angular acceleration caused by thrust
$\dot{q}_{\mathrm{uc}}$ = desired pitching angular acceleration caused by all control effectors
$\dot{q}_0$ = pitching angular acceleration produced only by the flight state
R_f = distance from the center of gravity to the lift-fan nozzle (V-1 aircraft)
R_v = distance from the center of gravity to the three bearing swivel duct nozzle (V-1 aircraft)
S = area of the wing
s = flag used in the optimization algorithm
T = rotor thrust (tilt rotor aircraft), step time
$T_{f\max}$ = maximal thrust of the lift-fan nozzle (V-1 aircraft)
T_t = unconstrained map of constrained T
$T_{v\max}$ = maximal thrust of the three bearing swivel duct nozzle (V-1 aircraft)
V = vehicle velocity
V_{xg} = component of velocity in the earth-fixed reference frame x axis
$V_{x\mathrm{gc}}$ = reference value of V_{xg}
V_{zg} = component of velocity in the earth-fixed reference frame z axis
$V_{z\mathrm{gc}}$ = reference value of V_{zg}
v_i = induced velocity (tilt rotor aircraft)
α = angle of attack
β = longitudinal disk tilt angle (tilt rotor aircraft)
γ = flight path angle
δ_a = aileron deflection

Received 1 December 2006; revision received 13 November 2007; accepted for publication 14 November 2007.

*Ph.D. Student, Department of Computer Science and Technology, 1-510 FIT Building, Mailbox 1303-15, 100073 Beijing; yang-xl03@mails.tsinghua.edu.cn.
†Ph.D. Student, Department of Computer Science and Technology, 811 Main Building; fan-y05@mails.tsinghua.edu.cn.
‡Professor, Department of Computer Science and Technology, 813 Main Building; jhzhu@mail.tsinghua.edu.cn.

δ_c = canard deflection (V-1 aircraft)
δ_{CD} = random function for uncertainty
δ_{CL} = random function for uncertainty
δ_{Cm} = random function for uncertainty
δ_e = elevator deflection
δ_f = pitch angle of the lift-fan nozzle (V-1 aircraft)
δ_{fT} = ratio of the lift-fan thrust to the maximal lift-fan thrust (V-1 aircraft)
δ_r = rudder deflection
δ_{Tl} = thrust of the left roll nozzles (V-1 aircraft)
δ_{Tr} = thrust of the left and right roll nozzles (V-1 aircraft)
δ_{vq} = pitch angle of the three bearing swivel duct nozzle (V-1 aircraft)
δ_{vr} = yaw angle of the three bearing swivel duct nozzle (V-1 aircraft)
δ_{vT} = ratio of the three bearing swivel duct nozzle thrust to the maximal three bearing swivel duct nozzle thrust (V-1 aircraft)
$\varepsilon_1, \varepsilon_2$ = positive constants used in the optimization algorithm
θ = pitch angle
θ_c = reference value of the pitch angle
θ_t = unconstrained map of constrained θ
θ_{1s} = longitudinal cyclic pitch (tilt rotor aircraft)
θ_{75} = collective pitch (tilt rotor aircraft)
ξ = angle from the horizontal line to the rotor thrust (tilt rotor aircraft), damping ratio
ρ = air density
ϕ = roll angle
ψ = yaw angle
ω_n = natural frequency

I. Introduction

THERE have been many types of vertical/short takeoff and landing (V/STOL) aircraft tested over the past 50 years [1]. Notable V/STOL aircraft include the Harrier, powered by a vectored-thrust engine; the Yak-38 Forger, equipped with two in-line lift engines and one turbojet with vectoring nozzles; the Bell XV-15 tilt rotor aircraft; the Bell–Boeing V-22 Osprey tilt rotor aircraft; and the X-35B (winner of the Joint Strike Fighter (JSF) program), equipped with a vectored-thrust engine and lift fan. Each of these aircraft belong to one of two categories. The first category is based on general jet aircraft equipment with components offering lift at low velocity; the other category is developed from the concept of the helicopter by tilting the rotor to form the propeller to achieve higher velocity.

Autonomous transition control of the VSTOL aircraft is an important challenge because the problem is different from general flight control problems. The two categories of VSTOL aircraft have many similar characteristics. This paper discusses the methodologies for the autonomous transition control, from hover to cruise, of two types of VSTOL aircraft. The first aircraft will be referred to as the V-1 aircraft, which has an engine configuration similar to the X-35B. The second aircraft is a tilt rotor aircraft. The two aircraft have the following common properties during transition flight mode: 1) both transition controls are nonlinear, nonaffine control problems; 2) both engine thrust and aerodynamic forces affect attitude and position movements directly; 3) the flight path angle must be controlled during transition; and 4) both transition control problems are multi-input problems and have special inputs, such as the engine nozzle pitch angle and the nacelle angle, that must reach specified end values after the transition process.

In this paper we propose two methods based on dynamic inversion to control the two aircraft, and we provide a comparison and analysis of them.

Traditional flight control methods such as gain scheduling are important in actual control system design [2]. However, the dynamic inversion method has gained more and more attention in aircraft flight control [3–5]. As the control problems in this paper are multi-input/multi-output and the number of inputs is more than the number of outputs, direct inversion cannot be applied. Therefore, a control allocation algorithm was applied to compute the values of the control inputs.

A simple daisy chain control allocation approach is adopted in Enns et al. [4]. It designates primary effectors for each of the three aircraft axes and treats other controls as auxiliary effectors to be used only when the primaries saturate. The control allocation problems are formulated as linear programs (LP) in Doman and Ngo [6]. To begin the process, a control strategy is achieved by an LP approach subject to the input position and rate constraints, and then a second LP is used to minimize a performance index that drives the control effectors into a preferred position. A nonlinear programming based control allocation scheme is developed in Poonamallee et al. [7]. First, the approach fits the aerodynamic data curve between the effector deflections and the moment coefficients with a polynomial approximation. Then it searches the effector deflections with a gradient-based nonlinear programming optimization. In Bolender and Doman [8], a piecewise linear programming approach is presented for the control allocation problem in which the controlled variable rates or moments are nonlinear functions of the effector deflections. This is because aerodynamic databases are discretely valued and almost always stored in multidimensional lookup tables, where it is assumed that the data are connected by piecewise linear functions. A model predictive, dynamic control allocation algorithm is developed in Luo et al. [9]. Unlike most existing algorithms neglecting the actuator dynamics or dealing with the actuator dynamics separately, the algorithm proposed in the paper directly takes the actuators dynamics into account. Petersen and Bodson [10] propose an interior-point algorithm to solve a mixed 12-norm optimization that is converted to a quadratic programming formulation. All of these papers discuss the attitude control of fixed-wing aircraft or space vehicles. V/STOL aircraft have stronger nonlinearities with nonlinear functions such as trigonometric functions, and the systems are nonaffine because the product of the functions of two inputs are in the mathematical model. In addition, both attitude and position should be controlled during transition flight. For the V-1 aircraft, a method is applied whose key point is that a new controlled variable is appended to decrease the redundancy of the control inputs. Aerodynamic surfaces are allocated with a daisy chain allocation approach described in Enns et al. [4] to control attitude. For the tilt rotor aircraft, we find that the first method is not appropriate because the V-1 aircraft can be controlled to rapidly increase velocity and pitch angle simultaneously, whereas the tilt rotor aircraft cannot, because the inputs required to produce linear and angular acceleration are conflicting when the aircraft starts transition flight from hover to forward flight. We therefore transfer the problem into a two-time-scale problem. Velocity is controlled by the outer loop, whereas attitude is controlled by the inner loop. Attitude is used as a control input to the outer loop. Nonlinear optimization is adopted in the outer loop to make the nacelle angle approach the desired end value. Because the system is nonaffine in the nacelle angle, we cannot use a single linear system to simplify the entire nonlinear system at all nacelle angles. Therefore, we cannot use the linear programming method described in Doman and Ngo [6] to achieve the task of driving the nacelle angle toward the desired value. In the inner loop, control allocation is scheduled as a function of dynamic pressure.

Two types of ideas about control input position and rate saturation were discussed in previous papers. In [6–8,10,11], the allocation algorithms designate control inputs based on their control capabilities by taking effector saturation into account directly. If the allocation algorithms could not achieve the desired dynamics, even if all control inputs reach saturation, the desired dynamics or the reference model was adjusted to adapt to the capabilities of the control effectors. The reference model was continually modified to fully use the available control capabilities [12]. Pseudocontrol hedging is adopted in Kannan and Johnson [13] to modify the reference model to prevent the difference between the commands to the control inputs and actual control inputs from driving an adaptive process into instability. Both [12,13] discuss the problems with control affine nonlinear models. In this paper, we use both ideas to deal with effector saturation. In the outer loop of the tilt rotor aircraft,

nonlinear programming with constraints is applied to enforce saturation limits. We detect axis saturation and use precalculated data to confine the output of the feedback control law to guarantee that the control variable rates can be achieved.

Neural network augmented model inversion control is applied to the tilt rotor aircraft longitudinal and lateral attitude control in [14,15], respectively. In this approach, a linear model of the helicopter mode is invested to attain control effector inputs, and then a neural network is used to compensate for inversion error. However, the control of the transition flight and multi-input characteristics of the tilt rotor aircraft are not discussed.

In [16,17], a tilt rotor flight control system is designed using the linear and nonlinear model predictive control methods, respectively. Multi-input characteristics are again not discussed.

In this paper, the problems are discussed and organized in the following way. Section II gives the longitudinal model of the V-1 aircraft and a mathematical model of the tilt rotor aircraft from Yang et al. [18] is repeated here. Section III presents the two methods of controlling the two aircraft. Section IV provides the results of the digital simulations. Conclusions are presented in Sec. V.

II. Mathematical Model

A. Model of the V-1 Aircraft

First, we present the model of the V-1 aircraft, which is equipped with an engine layout similar to the X-35B.

The X-35B JSF fighter has a JSF119-611 engine that has a three bearing swivel duct (3BSD) providing the aft post with axial thrust and vectored-thrust capability in pitch and yaw. The lift fan provides augmented thrust on the forward post. A set of roll ducts is used for lateral control. As shown in Fig. 1, the 3BSD nozzle can turn from 0 to 95 deg on the pitch axis, as well as from −12 to 12 deg on the yaw axis; the lift-fan nozzle can turn from 34 to 95 deg on the pitch axis [19].

The control inputs of the aircraft include δ_{vT}, δ_{vq}, δ_{vr}, δ_{fT}, δ_f, δ_{Tl}, δ_{Tr}, δ_a, δ_r, δ_c, and δ_e. All the actuator dynamics are second order with position and rate saturation constraints. The actuator characteristics are described in Table 1 in which ξ is the damping ratio and ω_n is the natural frequency.

Only a longitudinal model of the V-1 aircraft is presented in the paper. Figure 2 shows the longitudinal forces and moments acting on the V-1 aircraft.

The model can be stated as

$$\begin{cases} \dot{\theta} = q \\ \dot{q} = \frac{1}{I_{yy}}\left[-T_{v\max}\delta_{vT}R_v \sin\delta_{vq} + T_{f\max}\delta_{fT}R_f \sin\delta_f + \frac{1}{2}\rho V^2 S\bar{c}C_m(H,M,\alpha,q,\delta_e,\delta_c)\right] \\ \dot{V}_{xg} = \frac{1}{m}\left[(T_{f\max}\delta_{fT}\cos\delta_f + T_{v\max}\delta_{vT}\cos\delta_{vq})\cos\theta - (T_{f\max}\delta_{fT}\sin\delta_f + T_{v\max}\delta_{vT}\sin\delta_{vq}\cos\delta_{vr})\sin\theta - \frac{1}{2}\rho V^2 S C_D(H,M,\alpha,\delta_e,\delta_c)\cos\gamma - \frac{1}{2}\rho V^2 S C_L(H,M,\alpha,\delta_e,\delta_c)\sin\gamma\right] \\ \dot{V}_{zg} = \frac{1}{m}\left[-(T_{f\max}\delta_{fT}\cos\delta_f + T_{v\max}\delta_{vT}\cos\delta_{vq})\sin\theta - (T_{f\max}\delta_{fT}\sin\delta_f + T_{v\max}\delta_{vT}\sin\delta_{vq}\cos\delta_{vr})\cos\theta + \frac{1}{2}\rho V^2 S C_D(H,M,\alpha,\delta_e,\delta_c)\sin\gamma - \frac{1}{2}\rho V^2 S C_L(H,M,\alpha,\delta_e,\delta_c)\cos\gamma\right] + g \end{cases} \tag{1}$$

The aerodynamic data is obtained from a table and varies with Mach number, height, and angle of attack.

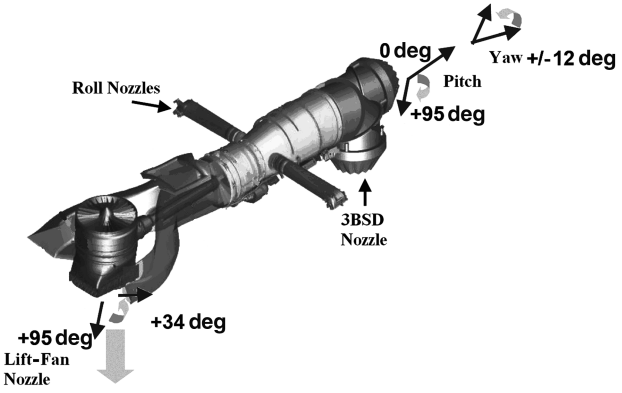

Fig. 1 X-35B engine layout.

It can be concluded from Eq. (1) that thrust affects both position and attitude movements in contrast to general jet aircraft, in which the main function of thrust is to regulate velocity.

The controlled variable for the V-1 is designated to be the flight path angle γ. It can be expressed as

$$\gamma = \arctan\left(\frac{-V_{zg}}{V_{xg}}\right) \tag{2}$$

The system (1) and (2) is a nonlinear, nonaffine, nonanalytic, and multi-input system. It has two special control inputs. They are the pitch angle of the 3BSD nozzle and the lift-fan thrust. They should arrive at specified end values to achieve transition from hover to forward flight.

B. Model of the Tilt Rotor Aircraft

Figure 3 shows the longitudinal forces and moments acting on the tilt rotor aircraft. The longitudinal nonlinear model of the tilt rotor can be expressed as

$$\begin{cases} \dot{\theta} = q \\ \dot{q} = \frac{1}{I_{yy}}\{-F_{Txb}l_3 \sin n + F_{Tzb}(l_1 - l_3\cos n) + m_A\} \\ \dot{V}_{xg} = \frac{1}{m}[F_{Txb}\cos\theta + F_{Tzb}\sin\theta - D_A\cos\gamma - L_A\sin\gamma] \\ \dot{V}_{zg} = \frac{1}{m}[-F_{Txb}\sin\theta + F_{Tzb}\cos\theta + D_A\sin\gamma - L_A\cos\gamma] + g \end{cases} \tag{3}$$

where

$$\begin{cases} F_{Txb} = T\cos(n-\beta) \\ F_{Tzb} = -T\sin(n-\beta) \end{cases} \tag{4}$$

$$\begin{cases} L_A = L_A(H,V,\alpha,q,\delta_e,v_i) = \frac{1}{2}\rho(V+v_i)^2 S C_L(H,M,\alpha,q,\delta_e,v_i) \\ D_A = D_A(H,V,\alpha,q,\delta_e,v_i) = \frac{1}{2}\rho(V+v_i)^2 S C_D(H,M,\alpha,q,\delta_e,v_i) \\ m_A = m_A(H,V,\alpha,q,\delta_e,v_i) = \frac{1}{2}\rho(V+v_i)^2 S\bar{c}C_m(H,M,\alpha,q,\delta_e,v_i) \end{cases} \tag{5}$$

Table 1 Effector characteristics of the V-1 aircraft

Effector	ξ	ω_n	Position limit	Rate limit
δ_e	0.8	34	[−30, 25] deg	±30 deg/s
δ_c	0.8	34	[−40, 10] deg	±30 deg/s
δ_a	0.8	40	[−20, 20] deg	±40 deg/s
δ_r	0.8	50	[−30, 30] deg	±40 deg/s
δ_{vT}, δ_{fT}	1	10	[0, 1]	±0.4
δ_{vq}	1	10	[0, 95] deg	±40 deg/s
δ_{vr}	1	10	[−12, 12] deg	±40 deg/s
δ_f	1	10	[34, 95] deg	±40 deg/s
δ_{Tl}, δ_{Tr}	1	10	[0, 10,000] N	±4000 N/s

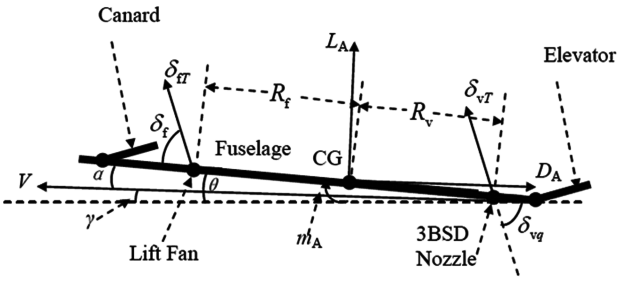

Fig. 2 Longitudinal forces and moments acting on the V-1 aircraft.

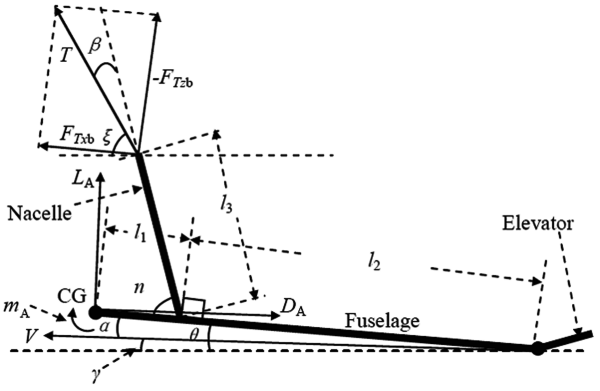

Fig. 3 Longitudinal forces and moments acting on the tilt rotor aircraft.

In Eq. (5), v_i is the induced velocity caused by rotors. According to Yang et al. [18], we can calculate β, T, and v_i using blade element theory and momentum theory. They can be expressed as

$$[\beta \;\; T \;\; v_i] = R(V_{xg}, V_{zg}, \theta, n, \theta_{75}, \theta_{1s}) \tag{6}$$

where θ_{75} is the blade collective pitch and θ_{1s} is the longitudinal cyclic pitch.

In Yang et al. [18], a gimbaled rotor model is explained by blade element theory and momentum theory.

The aerodynamic data is obtained from a table and varies with Mach number, height, and angle of attack.

The actuator characteristics are described in Table 2.

Similar to the V-1 aircraft already discussed, the tilt rotor model is also nonlinear, nonaffine, nonanalytic, and multi-input. Here the rotor thrust also affects both position and attitude movements, and the controlled variable is also the flight path angle. The specified control input is the engine nacelle angle n, which should reach a specified end value to achieve the transition from hover to forward flight.

III. Control Strategies

The two systems have many common characteristics. In this section, two control strategies will be developed and applied to the two models described in Sec. II.

A. Control Method for the V-1 Aircraft

The basic idea of the first method is that a new controlled variable is appended to decrease the redundancy of the control inputs. The new controlled variables are V_{xg}, V_{zg}, and θ, which are chosen to replace the original controlled variable γ. The reference values for these variables are calculated by a trim algorithm.

Equation (1) shows that both thrust and aerodynamic forces cause linear acceleration of the aircraft. The 3BSD nozzle thrust and the lift-fan thrust balance the gravity of the aircraft at hover or low-speed conditions. If the pitch angle of the 3BSD nozzle and the thrust of the lift fan are zero, the weight of the aircraft can only be balanced by aerodynamic lift, which requires the aircraft to be in forward flight. Therefore, we first transfer the original controlled variable, γ, into new controlled variables, V_{xg} and V_{zg}. But it is not certain that the specified control inputs, the pitch angle of the 3BSD nozzle and the lift-fan thrust, will reach zero when the V_{xg} and V_{zg} requirements are achieved. This is because system (1) and (2) has redundant inputs and there are an infinite number of solutions (within control power limits) to track V_{xg} and V_{zg}. These solutions depend on different values of the state variable θ. To reduce the redundancy of the control inputs and make the specified inputs reach the specified end values, we take θ as a new controlled variable. Another reason for modifying controlled variables to V_{xg}, V_{zg}, and θ is that increasing aerodynamic lift requires increasing the angle of attack and these three variables define the angle of attack, that is, $\alpha = \theta - \arctan(-V_{zg}/V_{xg})$.

The reference values of the new controlled variables can be calculated by a trim algorithm. In Eq. (1), there are 11 variables including δ_{vq}, δ_{vT}, δ_f, δ_{fT}, δ_e, δ_c, γ, α, V_{xg}, V_{zg}, and θ. We can set δ_{vq} and δ_{fT} to zero and δ_f to 90 deg because they are the inputs with specified end values. γ is taken to be the command given by the pilot. V_{zg} can be written as a function of V_{xg} and γ and θ can be written as a function of α and γ. The remaining variables are δ_{vT}, δ_e, δ_c, α, and V_{xg}. In addition, we can assume we only use δ_c (or δ_e) to control attitude when the transition flight finishes; therefore, the free variables reduce to δ_{vT}, δ_c, α, and V_{xg}. But Eq. (1) just has three effective equations; we must give the value of one variable before trim calculation. We select α as the variable and constrain it to the effective range. The trim algorithm is then applied to compute δ_{vT}, δ_c, and V_{xg}. Upon specification of the value of γ, we can compute the value of V_{zg} and θ. The values of V_{xg}, V_{zg}, and θ are taken as the new reference values to be tracked by the control system. Because the attitude movement of aircraft can be achieved more quickly than the position movement, by specifying a larger angle of attack and consequently obtaining smaller V_{xg} and V_{zg} commands by trim algorithm, the transition process will be faster.

Next, a dynamic inversion based method is developed to control the three controlled variables. A conceptual block diagram of the dynamic inversion controller is shown in Fig. 4, in which δ_* represents all of the control inputs.

Figure 5 [6,20,21] shows the linear controller in Fig. 4. This linear controller structure is used to control both V_{xg} and V_{zg}; thus, only the V_{xg} control loop is shown. On the right-hand side of the figure, the dynamic inversion and control allocation module and the aircraft can be approximated as a bank of decoupled integrators. The constraint

Table 2 Effector characteristics of the tilt rotor aircraft

Effector	ξ	ω_n	Position limit	Rate limit
δ_e	0.8	34	$[-30, 30]$ deg	± 30 deg/s
θ_{75}	0.8	40	$[5, 35]$ deg	± 40 deg/s
θ_{1s}	0.8	40	$[-25, 25]$ deg	± 40 deg/s
n	0.8	40	$[0, 90]$ deg	± 4.5 deg/s

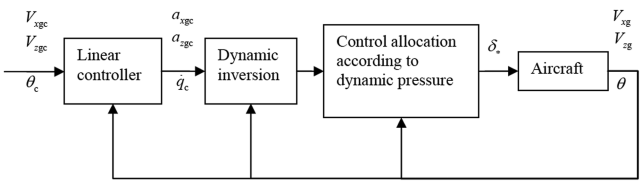

Fig. 4 Block diagram of the dynamic inversion controller.

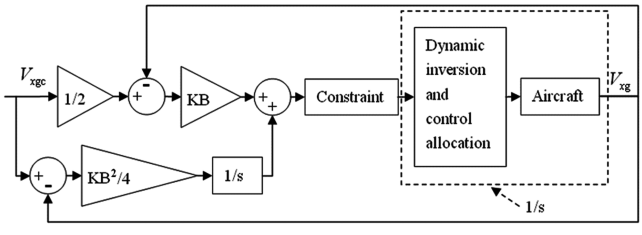

Fig. 5 Linear controller of the dynamic inversion.

element limits the desired acceleration to a physically realizable range, which helps ensure that the control allocator can generate control input solutions that do not violate rate or position limits. During transition from hover to level flight, the constraint element represents a simple saturation element that can guarantee that the control input solution will not violate rate or position limits. The saturation value can be derived from precalculation or test. But during the transition from level flight to hover, the constraint element is more complex and must be calculated according to the flight state.

The anticipated closed loop system dynamics is a first order system:

$$\frac{KB/2}{s+KB/2} \tag{7}$$

In addition, the pitch angle dynamics is second order so that the combination of the inversion module, control allocation module, and the aircraft pitch attitude dynamics can be approximately treated as a dual integrator system. A proportional integral derivative (PID) linear controller can be applied here to meet the control objective.

After the linear controller generates the desired linear acceleration $a_{x\mathrm{gc}}, a_{z\mathrm{gc}}$, and angular acceleration $\dot{q}_c$, control inputs to achieve these accelerations are computed by the inversion and control allocation module.

For simplification, the effect of the aerodynamic control surfaces on linear acceleration is neglected in the control design; however, they are included in the simulation model. There are three reasons to neglect the effect of the aerodynamic control surfaces on linear acceleration. First, at low dynamic pressure, the effect of the aerodynamic control surfaces is trivial. Second, at high dynamic pressure, the effects of the aerodynamic control surfaces on linear acceleration are small enough to be canceled by incorporating integrators into the control law. Snell et al. [3] presents an analysis of the canard effect on slow states and concludes that the effect is negligible. And third, the elevator that is aft the center of gravity of the aircraft will contribute to nonminimum phase behavior. For nonminimum phase systems, a direct inversion leads to internally unstable control laws. By direct inversion, upward acceleration requires the elevator downward deflection, but downward deflection of the elevator will cause downward acceleration in the long run by decreasing the angle of attack. For this reason, we do not compute the values of surface deflection by inversion. The effect of the aerodynamic force due to control surfaces is considered as a disturbance, just like uncertainty on the aerodynamic coefficients. Papageorgiou and Glover [21] compared the robust stability and robust performance of two dynamic inversion linear control laws for the F/A18, when uncertainty on the aerodynamic coefficients is taken into account. One is a proportional controller; the other is a proportional-plus-integral controller that is used in this paper (Fig. 5). With the proportional integral controller, a larger region of attraction is guaranteed and the performance is better for uncertainty, suggesting that the presence of the integrator is beneficial. In Sec. IV, we present uncertainty on the aerodynamic coefficients in the simulation model to test the robustness of the controller.

F_{Txb} and F_{Tzb} are components of the sum of the lift fan and 3BSD nozzle thrust in the body x and z axis. They can be expressed as

$$\begin{cases} T_{f\max}\delta_{fT}\cos\delta_f + T_{v\max}\delta_{vT}\cos\delta_{vq} = F_{Txb} \\ -(T_{f\max}\delta_{fT}\sin\delta_f + T_{v\max}\delta_{vT}\sin\delta_{vq}\cos\delta_{vr}) = F_{Tzb} \end{cases} \tag{8}$$

Substituting $a_{x\mathrm{gc}}$ and $a_{z\mathrm{gc}}$ into Eq. (1), we attain

$$\begin{cases} ma_{x\mathrm{gc}} + \frac{1}{2}\rho V^2 S C_D(H,M,\alpha,0,0)\cos\gamma \\ \quad + \frac{1}{2}\rho V^2 S C_L(H,M,\alpha,0,0)\sin\gamma = F_{Txb}\cos\theta + F_{Tzb}\sin\theta \\ ma_{z\mathrm{gc}} - \frac{1}{2}\rho V^2 S C_D(H,M,\alpha,0,0)\sin\gamma \\ \quad + \frac{1}{2}\rho V^2 S C_L(H,M,\alpha,0,0)\cos\gamma - mg \\ = -F_{Txb}\sin\theta + F_{Tzb}\cos\theta \end{cases} \tag{9}$$

Substituting the flight state values into Eq. (9), we can obtain the desired F_{Txb} and F_{Tzb}.

With the expression of $\dot{q}$ in Eq. (1), we can obtain the control inputs required to produce the desired angular acceleration, $\dot{q}_c$. The angular acceleration that will be produced by control inputs can be expressed as

$$\begin{aligned} \dot{q}_{\mathrm{uc}} = \dot{q}_c - \dot{q}_0 = \frac{M_T}{I_{yy}} + \frac{\rho V^2 S\bar{c}}{2I_{yy}}[C_m(H,M,\alpha,q,\delta_e,\delta_c) \\ - C_{m0}(H,M,\alpha) - C_{mq}(H,M)q] = \frac{M_T}{I_{yy}} \\ + \frac{\rho V^2 S\bar{c}}{2I_{yy}}[C_{m\delta_e}(H,M,\alpha)\delta_e + C_{m\delta_c}(H,M,\alpha)\delta_c] = \dot{q}_{Tc} + \dot{q}_{\mathrm{ac}} \end{aligned} \tag{10}$$

where $\dot{q}_0$ is the angular acceleration produced only by the flight state and M_T is the moment generated by the engine.

Because angular acceleration depends on both thrust-based and aerodynamic effectors, it is necessary to schedule these effectors as a function of dynamic pressure. At low dynamic pressure, the force and moment contributions from the aerodynamic control surfaces can be neglected while the thrust-based effectors are dominant; thus, we rely upon thrust-based effectors to deliver the required angular acceleration, that is, $\dot{q}_{Tc} \triangleq \dot{q}_{\mathrm{uc}}$, $\dot{q}_{\mathrm{ac}} \triangleq 0$. At high dynamic pressure, the situation is reversed and we rely upon the aerodynamic surfaces to deliver the commanded angular acceleration, that is, $\dot{q}_{Tc} \triangleq 0$, $\dot{q}_{\mathrm{ac}} \triangleq \dot{q}_{\mathrm{uc}}$. During the transition from hover to forward flight, the thrust-based and aerodynamic control effectors must be blended to achieve the desired pitch acceleration. The overall allocation scheme is described as

$$\begin{cases} \dot{q}_{\mathrm{ac}} = 0; \dot{q}_{Tc} = \dot{q}_{\mathrm{uc}}, & 0 \le V < 30 \text{ m/s} \\ \dot{q}_{\mathrm{ac}} = \dot{q}_{\mathrm{uc}}(V-30)/30; \dot{q}_{Tc} = \dot{q}_{\mathrm{uc}} - \dot{q}_{\mathrm{ac}}, & 30 \text{ m/s} \le V < 60 \text{ m/s} \\ \dot{q}_{\mathrm{ac}} = \dot{q}_{\mathrm{uc}}; \dot{q}_{Tc} = 0, & V \ge 60 \text{ m/s} \end{cases} \tag{11}$$

In this paper, a daisy chain allocation method [4] is adopted to designate the elevator and canard with consideration of the position and rate saturation. It designates the canard to achieve pitch acceleration first. The elevator is treated as an auxiliary effector to be used only when the canard saturates.

The moment generated by engine is given by

$$-T_{v\max}\delta_{vT}R_v\sin\delta_{vq}\cos\delta_{vr} + T_{f\max}\delta_{fT}R_f\sin\delta_f = \dot{q}_{Tc}I_{yy} = M_T \tag{12}$$

With Eqs. (8) and (12), keeping $\delta_f = 90$ deg, we can obtain δ_{vT}, δ_{vq}, and δ_{fT}.

B. Control Method for the Tilt Rotor Aircraft

The tilt rotor aircraft model given in Eq. (3) has two kinds of separate longitudinal control inputs. The first type is provided by the rotors, including blade collective pitch, longitudinal cyclic pitch, and nacelle angle. The second type is the aerodynamic control surface, including the elevator. The nacelle angle should be zero when the transition finishes. For the same reasons as the V-1 aircraft, the influence of the aerodynamic surfaces to the linear acceleration is neglected. However, to demonstrate the validity of the result with more realistic conditions, the nonminimum phase effects of the elevator on the flight path angle are taken into account in the simulation model. Uncertainty on aerodynamic coefficients is also included in the model.

The method applied to the V-1 does not work for the tilt rotor aircraft. Similar to the V-1 aircraft, the velocity and angle of attack should be increased to produce aerodynamic lift. However, the linear acceleration and angular acceleration are conflicting when a tilt rotor aircraft initiates the transition to forward flight from hover. Tilt rotor aircraft can accelerate with a constant pitch attitude from hover by

rotating the nacelles forward and tilting the disk plane backward relative to the nacelles to maintain the longitudinal moment at zero. However, this results in small linear accelerations. If the aircraft is commanded to pitch up, the disk plane must tilt backward much more to produce the required pitching moment, and the linear acceleration is much smaller. Increasing linear acceleration will decrease angular acceleration and vice versa. Consequently, if linear and angular acceleration are demanded simultaneously, they must both be very small. Therefore, tilt rotor aircraft are different from thrust vectored aircraft like the V-1, which can simultaneously accelerate and pitch up rapidly. To solve this problem, we propose another approach to control the transition flight of the tilt rotor aircraft.

First, we transfer the problem into a two-time-scale problem based on singular perturbation theory.

The outer loop is the velocity loop and the inner loop is the attitude loop. The controlled variables of the outer loop are V_{xg} and V_{zg}. The pitch angle is considered as a control input to the outer loop, and it is controlled by the inner loop. The dynamic inversion method is used to control both outer and inner loops. Figure 6 shows the block diagram of the inner- and outer-loop controllers. After the linear controller of the outer loop obtains the desired linear accelerations, the inversion and control allocation module calculates the control inputs of the outer loop with a constrained optimization method (e.g., linear programming, nonlinear programming) to make the input n reach its specified value more rapidly. The position and rate saturation of all of the controls can be taken into account using this method.

Because of the complexity of the rotor system, the required T and β to achieve the desired linear and angular acceleration are calculated first. Then, according to the model of the rotor, we obtain the corresponding collective and cyclic pitch.

The linear controller of the outer loop is the same as described in Fig. 5. Taking $a_{x\mathrm{gc}}$ and $a_{z\mathrm{gc}}$ into Eq. (3), we can obtain the equations of motion for the longitudinal translational degrees of freedom:

$$\begin{cases} 0 = \frac{1}{m}[F_{Txb}\cos\theta + F_{Tzb}\sin\theta - D_A\cos\gamma - L_A\sin\gamma] - a_{x\mathrm{gc}} = \Delta a_{x\mathrm{gc}} \\ 0 = \frac{1}{m}[-F_{Txb}\sin\theta + F_{Tzb}\cos\theta + D_A\sin\gamma - L_A\cos\gamma] \\ \quad + g - a_{z\mathrm{gc}} = \Delta a_{z\mathrm{gc}} \end{cases} \tag{13}$$

This equation is used to obtain control inputs $[\theta \ \ \beta \ \ T \ \ n \ \ \delta_e]$ to achieve $a_{x\mathrm{gc}}$ and $a_{z\mathrm{gc}}$. Because Eq. (13) has only two equations but five variables, it is necessary to reduce the dimensions or add new constrained conditions to solve the problem.

Because the contribution to linear acceleration is slight, the elevator deflection δ_e is set to zero.

Based on Eq. (4), when β is at its maximal value, 11 deg, we can compute the influence of β on forces acting on the aircraft at a different nacelle angle. Figure 7 shows a comparison of forces acting on the body–axis system with $\beta = 0$ and $\beta = 11$ deg. We can see that when the aircraft is in helicopter mode, β will augment the force along the body x axis for about $0.2T$, but the force along the body z axis has little change. Therefore, one may conclude that β contributes little to linear acceleration, especially to vertical movement. The primary function of β is to produce a pitching moment. Because the usable range of β is maximized in helicopter mode, its influence on

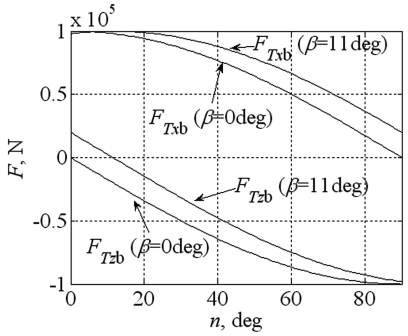

Fig. 7 Comparison of forces acting on the body–axis system with $\beta = 0$ and $\beta = 11$ deg ($T = 100,000$ N).

the linear acceleration is neglected in forward flight and β can be set to zero. The remaining free variables are $[\theta \ \ T \ \ n]$.

Because there is an end value constraint on the nacelle angle n, the task becomes solving for three variables with three equations and the solution is unique. Doman and Ngo [6] provide an LP method to drive the control surfaces toward a preferred position. The model of the tilt rotor aircraft has strong nonlinearities with trigonometric functions. The system is also nonaffine in nacelle angle. Therefore, we cannot use a single linear system to simplify the whole nonlinear system at all nacelle angles. This is the reason that the linear programming control allocation method cannot be applied to achieve the task of driving the nacelle angle toward the desired value.

Here, a two-layer search method is proposed to achieve optimization. Figure 8 shows the block diagram of this method.

The lower layer, n, is fixed to judge whether $a_{x\mathrm{gc}}$ and $a_{z\mathrm{gc}}$ can be achieved at a given value of n and to calculate the corresponding $[\theta \ \ T]$. Because Eq. (13) is nonlinear, nonaffine, and nonanalytic, a numerical method must be applied to solve the equation. In this paper, the Broyden–Fletcher–Goldfarb–Shanno (BFGS) method, a popular quasi-Newton algorithm [22], is adopted to solve the equation. The BFGS method not only has the advantage of the Newton method, which converges rapidly, but it also has a new H matrix updating method to replace the Hessian matrix used in the Newton method, which does not guarantee the Hessian matrix to be a positive definite.

There are several points to consider when using the BFGS method to solve Eq. (13):

1) Equation (13) or the actual aircraft is high-order differentiable, although it is nonanalytic.

2) Neural networks trained by experimentation can replace Eq. (3) in practice. The inputs of the backpropagation (BP) neural networks are the values of states and control inputs. The outputs of the neural networks are linear and angular acceleration, which can be calculated by forces and moments and measured by sensors. The neural networks can be trained using the results of many predesigned experiments.

3) The Jacobian matrix used in the algorithm can be obtained by the analytic derivative of the neural network or by calculating the output variation rate of the model with small perturbations.

4) With the following method, we can transfer Eq. (13) from constrained optimization to unconstrained optimization. We choose a continuous high-order differentiable function $\phi(x)$, whose domain

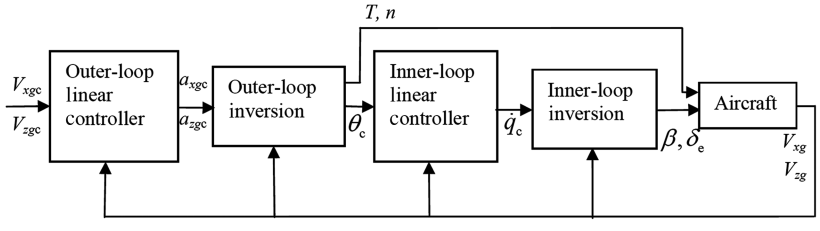

Fig. 6 Block diagram of the inner and outer loop of the tilt rotor aircraft controller.

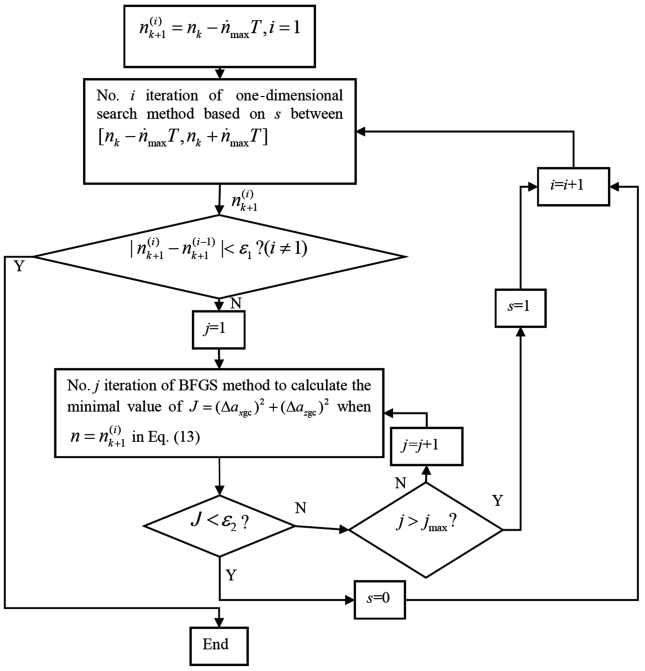

Fig. 8 Two-layer search method for optimization.

of definition is $(-\infty, \infty)$ and range of function is $[-1, 1]$, for example $\phi(x) = \sin(x)$. According to the range of θ and T, we can express them with $\phi(x)$. For example, if the range of θ is $(-a, a)$, then θ can be expressed as $\theta = a\phi(\theta_t)$, and if the range of T is (a, b), then T can be expressed as $T = [b + a + (b - a)\phi(T_t)]/2$. The BFGS method can be adopted to solve for θ_t and T_t. Accordingly, we compute θ and T from θ_t and T_t.

5) To solve Eq. (13), we choose the objective function as $J = (\Delta a_{xgc})^2 + (\Delta a_{zgc})^2$.

6) Set a maximum allowed iteration number $j_{\max}$. If the iteration number exceeds this number and the value of the objective function is larger than a given positive constant ε_2, then Eq. (13) is viewed as no solution at current n.

On the higher layer, a one-dimensional search method is applied to obtain an optimized n command of the current step in the range $[n_k - \dot{n}_{\max}T, n_k + \dot{n}_{\max}T]$, where n_k is the nacelle angle at step k, T is the step time, and $\dot{n}_{\max}$ is the maximal nacelle angular velocity. In Fig. 8, the value of s determines the search direction. $s = 0$ represents that Eq. (13) has a solution, and then the algorithm searches for a smaller n to satisfy Eq. (13). $s = 1$ represents that Eq. (13) has no solution, and then the algorithm searches for a larger n to satisfy Eq. (13). $n_{k+1}^{(i)}$ represents the value of the number i iteration for the step $k + 1$. The result of the n command should be the nearest position to $n_k - \dot{n}_{\max}T$ (or $n_k + \dot{n}_{\max}T$ during the transition from fixed-wing mode to helicopter mode) with the constraint stated in Eq. (13) satisfied. When the difference of two iterations is less than a given positive constant ε_1, the one-dimensional search method finishes.

When the required θ command is calculated by the outer loop, it can be realized by the inner-loop controller. The inner-loop controller also uses dynamic inversion. The PID controller is adopted as the linear controller to produce the desired angular acceleration $\dot{q}_c$. $\dot{q}_{\text{uc}}$ is the desired angular acceleration to be produced by the control inputs. According to dynamic pressure, we can allocate $\dot{q}_{\text{uc}}$ to different control inputs with Eq. (14):

$$\begin{cases} \dot{q}_{Tc} = 0; \dot{q}_{\text{ac}} = \dot{q}_{\text{uc}}, & 0 \le n < 20 \text{ deg}, (V > 65 \text{ m/s}) \\ \dot{q}_{Tc} = \dot{q}_{\text{uc}}(n - 20)/40; \dot{q}_{\text{ac}} = \dot{q}_{\text{uc}} - \dot{q}_{Tc}, & 20 \le n < 60 \text{ deg} \\ \dot{q}_{Tc} = \dot{q}_{\text{uc}}; \dot{q}_{\text{ac}} = 0, & 60 \le n \le 90 \text{ deg}, (V < 20 \text{ m/s}) \end{cases} \tag{14}$$

With $\dot{q}_{\text{ac}}$ specified we can obtain

$$\delta_e = \frac{2I_{yy}\dot{q}_{\text{ac}}}{\rho V^2 S\bar{c}C_{m\delta_e}(H, M, \alpha)} \tag{15}$$

Substituting $\dot{q}_{Tc}$ into the second equation of Eq. (3), the following equation is obtained:

$$\dot{q}_{Tc} = \frac{1}{I_{yy}}[-F_{Txb}l_3 \sin n + F_{Tzb}(l_1 - l_3 \cos n)] \tag{16}$$

Taking T obtained by the outer-loop controller into Eq. (16), we can obtain β to achieve $\dot{q}_{Tc}$.

Using the rotor model described in Eq. (6) and selecting V_{xg}, V_{zg}, θ, n, θ_{75}, θ_{1s} randomly among their range, we can obtain the stable state induced velocity v_i, thrust T_h, and drag H_h in the hub axis. A BP neural network is trained to fit the inverse model of Eq. (6) from $[V_{xg}, V_{zg}, \theta, n, T_h, H_h]$ to $[\theta_{75}, \theta_{1s}]$. With the neural network, the required T_h and H_h can be solved from the required T and β; subsequently, $[\theta_{75}, \theta_{1s}]$ can be obtained from T_h and H_h. Neural network online training can decrease the error between experimental data and flight data as well as the error caused by neural network training.

During the transition flight of the tilt rotor aircraft, there is another problem that should be noted, that is, the control capability of the outer loop. Under some conditions, it is possible that the desired linear acceleration generated by the linear controller cannot be achieved. For example, when the aircraft is commanded to transform from fixed-wing level flight mode to hover mode, it must decelerate. The linear controller used to generate the reference acceleration is a first- or second-order controller just like Fig. 5, but the linear controller will provide a large deceleration command at the beginning of the transition. Such large deceleration commands cannot be achieved when the aircraft is in fixed-wing level flight mode. We refer to this phenomenon as axis saturation. The minimal and maximal horizontal acceleration available when maintaining vertical velocity and acceleration as zero are mainly determined by four variables, including V_{xg}, n, θ, and T. Using the nonlinear optimization algorithm, we obtain the minimal and maximal horizontal acceleration available with the constraint of θ and T at different V_{xg} and n. The range of θ is $(-29, 11$ deg). The range of T is (1000; 150,000 N). The result is shown in Fig. 9. The upper surface in Fig. 9a describes the maximal horizontal acceleration available. The lower surface describes the minimal horizontal acceleration available. The plane right-hand side of the figure describes the conditions at which vertical acceleration cannot be maintained at zero. Figure 9c shows the maximal and minimal horizontal acceleration available when the nacelle angle is zero. When velocity is lower than 70 m/s, the aircraft cannot maintain zero vertical acceleration. When the velocity is larger than 70 m/s, the horizontal deceleration available is small. Figure 9b shows the maximal and minimal horizontal acceleration available when the nacelle angle is 90 deg. It shows that the horizontal deceleration available is larger than when nacelle angle is zero. The linear controller should provide horizontal acceleration commands that lie in the feasible space between the two surfaces in Fig. 9a. We must therefore use the precalculated data in the constraint module shown in Fig. 5 to guarantee that the acceleration can be physically achieved.

Furthermore, we must consider the impact of the use of control power from the lateral-directional control law in a practical application. We can also apply the principles described in the paper when designing a multi-axis controller, however, modifications must be made. For the V-1 aircraft, the controlled variables would include

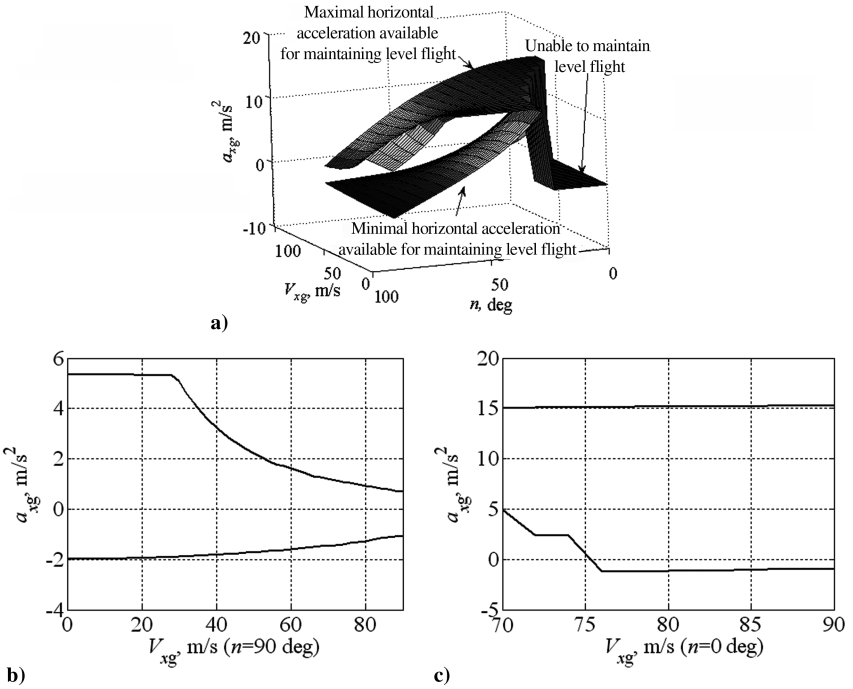

Fig. 9 Available horizontal acceleration at different V_{xg} and n.

γ, ϕ, and ψ, which would be translated into V_{xg}, V_{zg}, θ, ϕ, and ψ commands to eliminate redundancy. A more integrated control allocation method would be required to obtain multi-axis control inputs to allocate control power and to avoid saturation. For the tilt rotor aircraft, one could obtain θ, T, and n with the outer-loop controller by optimization algorithm, and then control θ, ϕ, and ψ with the inner-loop controller. A more integrated control allocation method would be required to obtain collective pitch, cyclic pitch, and aerodynamic effector deflection commands. When velocity is controlled, a principle for avoiding saturation is that $|a_{xgc}|$ may be decreased to guarantee that other controlled variable rates can be achieved. The reference dynamics of the controlled variables could also be adjusted online. A full discussion of the incorporation of lateral-directional control with the proposed longitudinal methods is beyond the scope of this paper.

IV. Simulation

This section gives the digital simulation results of the two control methods for the two aircraft. To assess the robustness of the controllers, uncertainty on aerodynamic coefficients is added to the simulation models used in this section. The uncertainty is represented in this form

$$\begin{cases} C_L = C_L(H, M, \alpha, \delta_e, \delta_c) + \hat{C}_L \delta_{CL} \\ C_D = C_D(H, M, \alpha, \delta_e, \delta_c) + \hat{C}_D \delta_{CD} \\ C_m = C_m(H, M, \alpha, q, \delta_e, \delta_c) + \hat{C}_m \delta_{Cm} \end{cases} \tag{17}$$

which is similar to that used in Papageorgiou and Glover [21].

$\hat{C}_L$, $\hat{C}_D$, and $\hat{C}_m$ are the maximal magnitude of the uncertainty. It is given by

$$\begin{cases} \hat{C}_L = |C_L(H, M, \alpha, \delta_{e\max}, 0) - C_L(H, M, \alpha, 0, 0)| \\ \hat{C}_D = |C_D(H, M, \alpha, \delta_{e\max}, 0) - C_D(H, M, \alpha, 0, 0)| \\ \hat{C}_m = 0.05|C_m(H, M, \alpha, q, \delta_{e\max}, 0) - C_m(H, M, \alpha, q, 0, 0)| \end{cases} \tag{18}$$

where $\delta_{e\max}$ is the maximal deflection of the elevator. In this way it is easier to quantify any uncertainty on the model by considering it as uncertainty on the pitching moment and force coefficients caused by change in the input variable. For the uncertainty magnitude on force coefficients $\hat{C}_L$, $\hat{C}_D$, we use the maximal change of coefficients caused by the elevator to assess robustness while ignoring the surface effect on force during the control design. For the uncertainty magnitude on moment coefficient $\hat{C}_m$, we cannot use the maximal change of coefficient caused by the elevator because the elevator is designed to produce pitch moment. Therefore, a positive number $c < 0.5$ is used to characterize the amount of uncertainty. A different value of c produces a different region of attraction. We use $c = 0.05$ in the paper.

δ_{CL}, δ_{CD}, and δ_{Cm} are random variables that provide uniformly distributed random numbers in the interval $(-1, 1)$. These variables are varied randomly at each simulation time step.

A. Simulation Results of the V-1 Aircraft

Figure 10 shows the simulation results of the V-1 aircraft maintaining level flight during the transition. The figure shows that the aircraft achieves the transition flight successfully. In this process, the aircraft accelerates from hover to level flight with a 65 m/s velocity and the angle of attack increases from zero to the value required to produce sufficient lift to balance the weight of the aircraft. During the transition flight, the aircraft maintains near-constant altitude. When the transition finishes, the thrust of the lift fan decreases to zero and the pitch angle of the 3BSD nozzle turns to 0 from 90 deg. Then, another controller for level flight is applied. At low velocity the engine controls the attitude movement, whereas at high velocity the canard is used as the primary pitch effector. For medium velocity, the engine and canard control the attitude synergistically. The simulation result shows that the controller is robust enough to deal with the aforementioned uncertainty and the effect caused by the nonminimum phase behavior.

Figure 11 shows the simulation results of the V-1 aircraft climbing from hover with a flight path angle of 2.9 deg during transition. The figure indicates that the controller achieves the transition flight successfully and is robust to the uncertainty.

B. Simulation Results of the Tilt Rotor Aircraft

Figure 12 shows the simulation results of the tilt rotor aircraft maintaining a constant altitude flight during transition. The maximal tilting angular velocity of the nacelle angle n is 4.5 deg/s. The aircraft is commanded to achieve the transition flight as fast as possible. The results show that the aircraft maintains level flight and finishes the transition flight within 20 s (transition starts at 10 s). The nacelles tilt to level at the consistent and maximal available angular

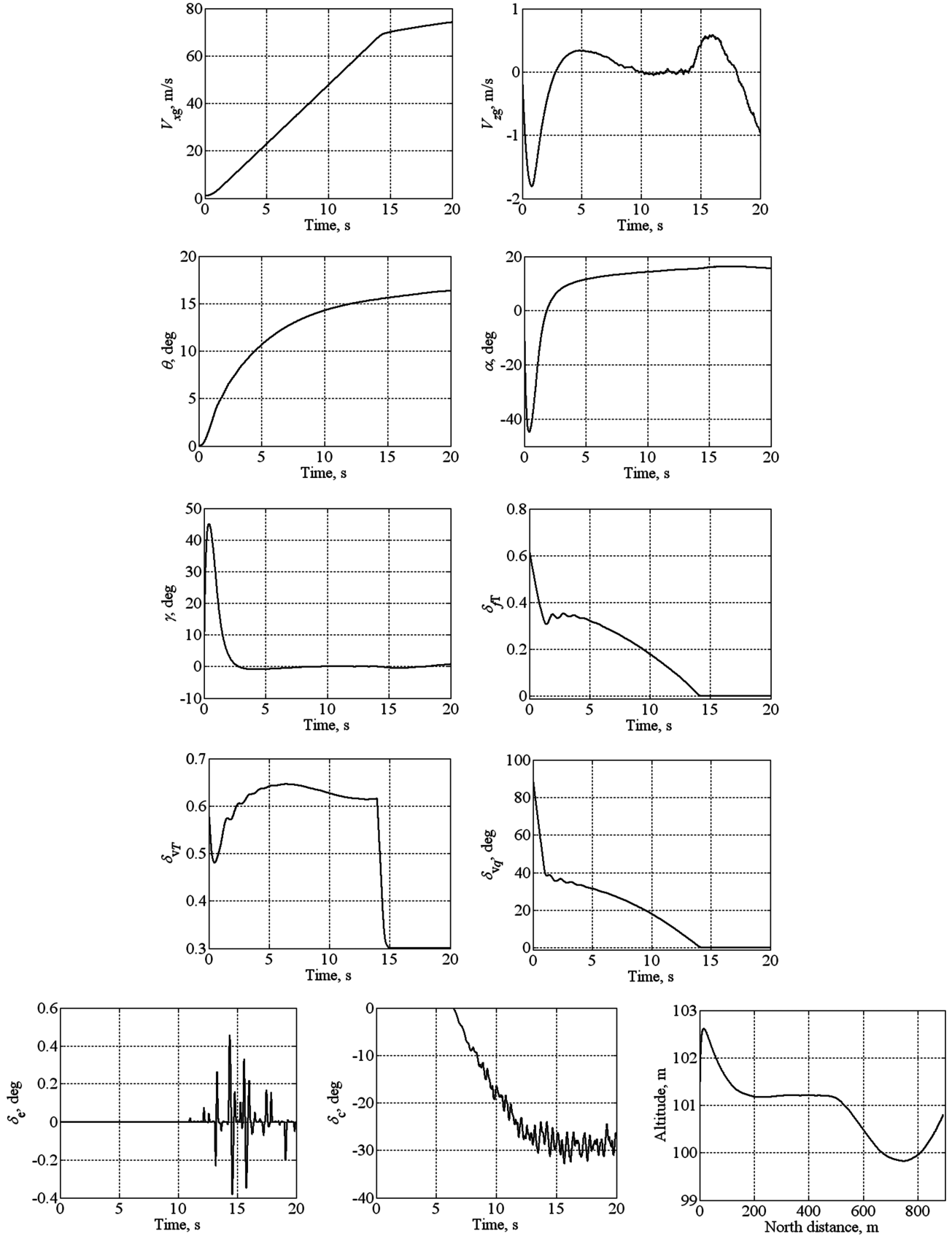

Fig. 10 Simulation results for the V-1 aircraft transitioning from hover with level flight.

velocity. The figure also indicates that when the aircraft accelerates from hover, its pitch angle decreases first. The last subplot of Fig. 12 shows the iteration number of the nonlinear optimization method and the numerical performance of the algorithm. The simulation results show that the controller is robust to the uncertainty.

When the aircraft is commanded to accelerate slowly, the nacelles cannot tilt to level at the consistent and maximal available angular velocity. Figure 13 shows the simulation results of this condition. It takes about 30 s for the aircraft to achieve the transition flight. This is because the rotor thrust cannot support the weight of the aircraft with

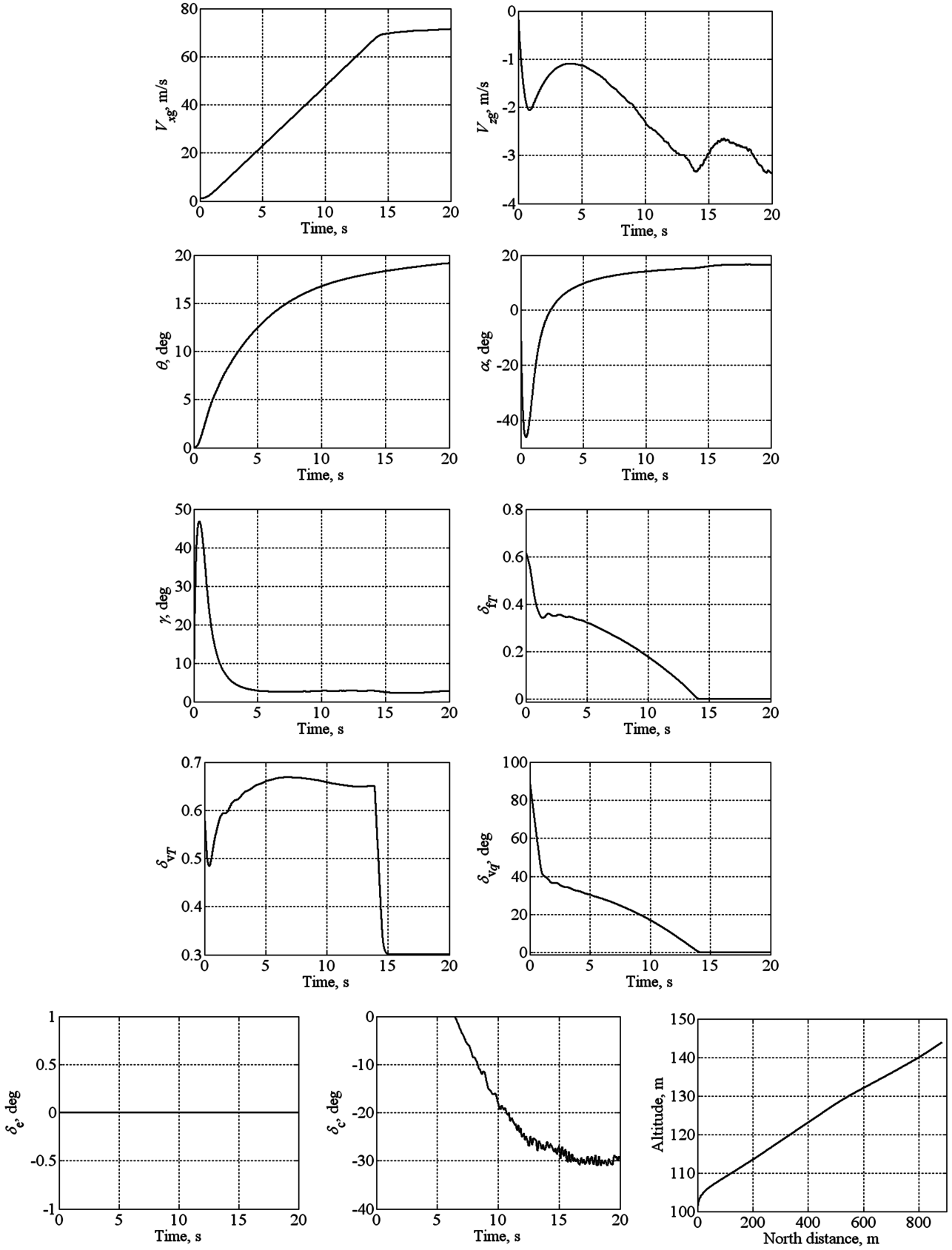

Fig. 11 Simulation results for the V-1 aircraft transitioning and climbing from hover.

a low aircraft velocity and small nacelle angle. At this condition, the controller can control the nacelle tilt at a different angular velocity based on the instantaneous aircraft velocity to achieve the transition flight safely. Figure 13 shows the merit of the control algorithm at this condition. The simulation results show that the controller is robust to the uncertainty.

Figure 14 shows the results of the simulation of the tilt rotor aircraft climbing from hover with a flight path angle of 5.7 deg during transition. The figure indicates that the controller achieves the transition flight successfully. Also, the angle of attack is constrained in the proper range to avoid stall. The simulation results show that the controller is robust to the uncertainty.

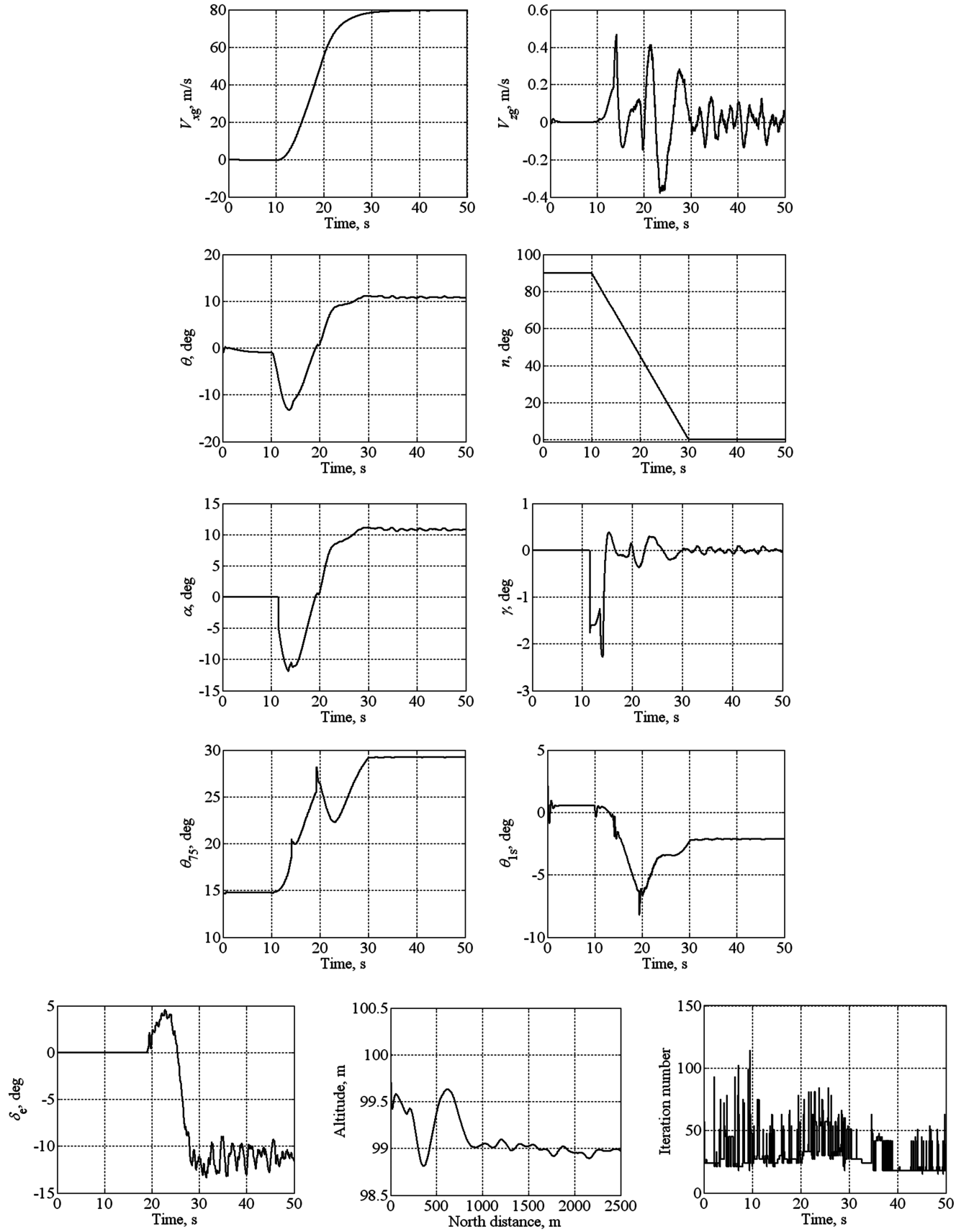

Fig. 12 Simulation results for tilt rotor transitioning from hover with level flight.

Figure 15 shows the results of the simulation of the tilt rotor aircraft maintaining level flight during transition from fixed-wing mode to helicopter mode. The initial velocity is 80 m/s and the horizontal velocity command is zero. The horizontal velocity cannot track the first-order reference dynamics because the desired deceleration cannot be achieved at a small nacelle angle. As a result, the horizontal acceleration is restricted within the minimal and maximal values shown in Fig. 9a. After the aircraft transforms into

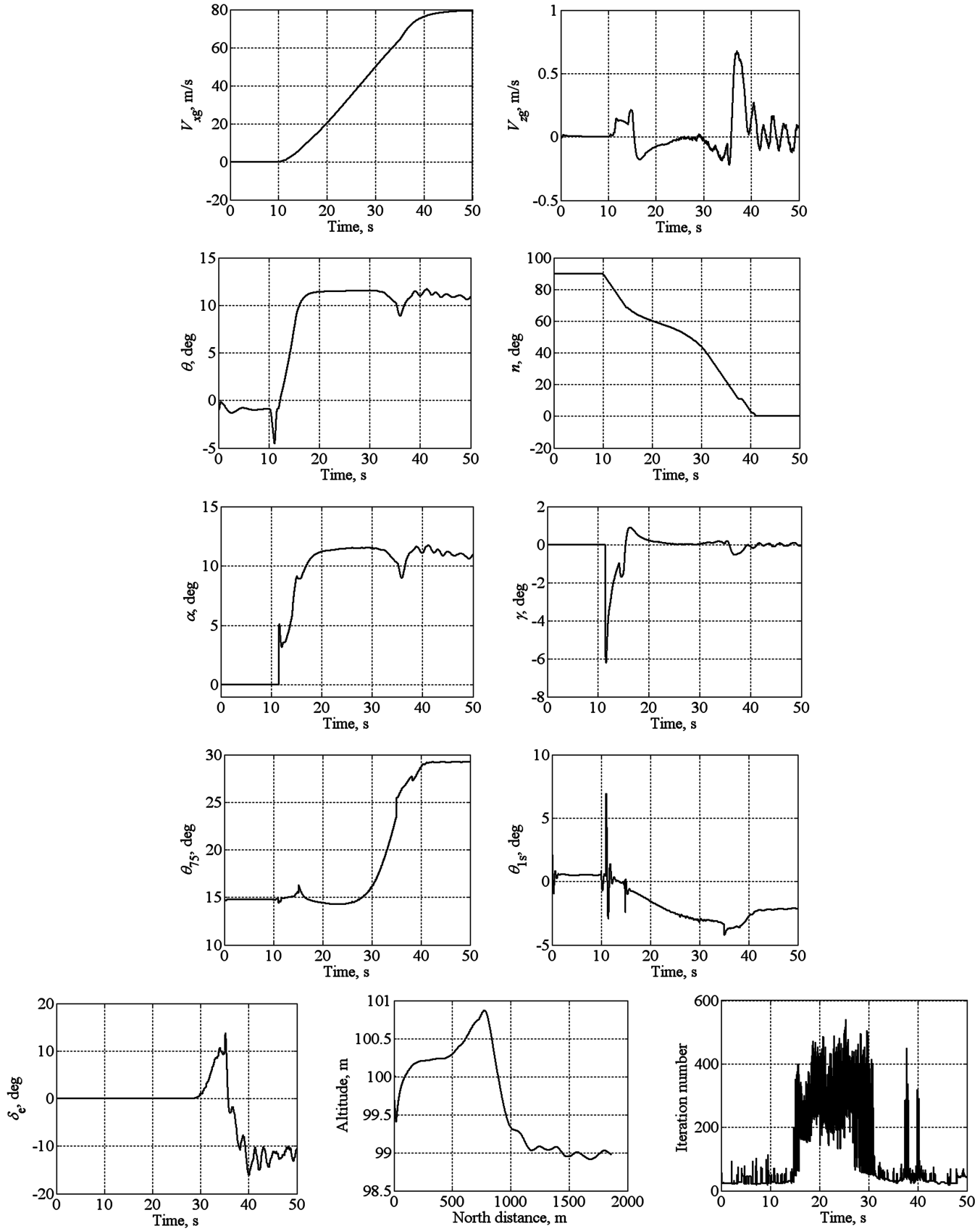

Fig. 13 Simulation results for tilt rotor transitioning from hover with low-acceleration level flight.

helicopter mode, a larger deceleration can be achieved. The aircraft does not decelerate by pitching up at the start because the range of the angle of attack is restricted below 11.5 deg; the pitch angle is also restricted below 11.5 deg. When the aircraft starts the transition, the pitch angle is close to 11.5 deg, and so the aircraft cannot pitch up excessively to decelerate. The simulation results show that the controller is robust to the uncertainty.

The last plot of these figures shows the iteration number of the nonlinear optimization method. The iteration number is the number of times that Eq. (13) is computed in the optimization process. In

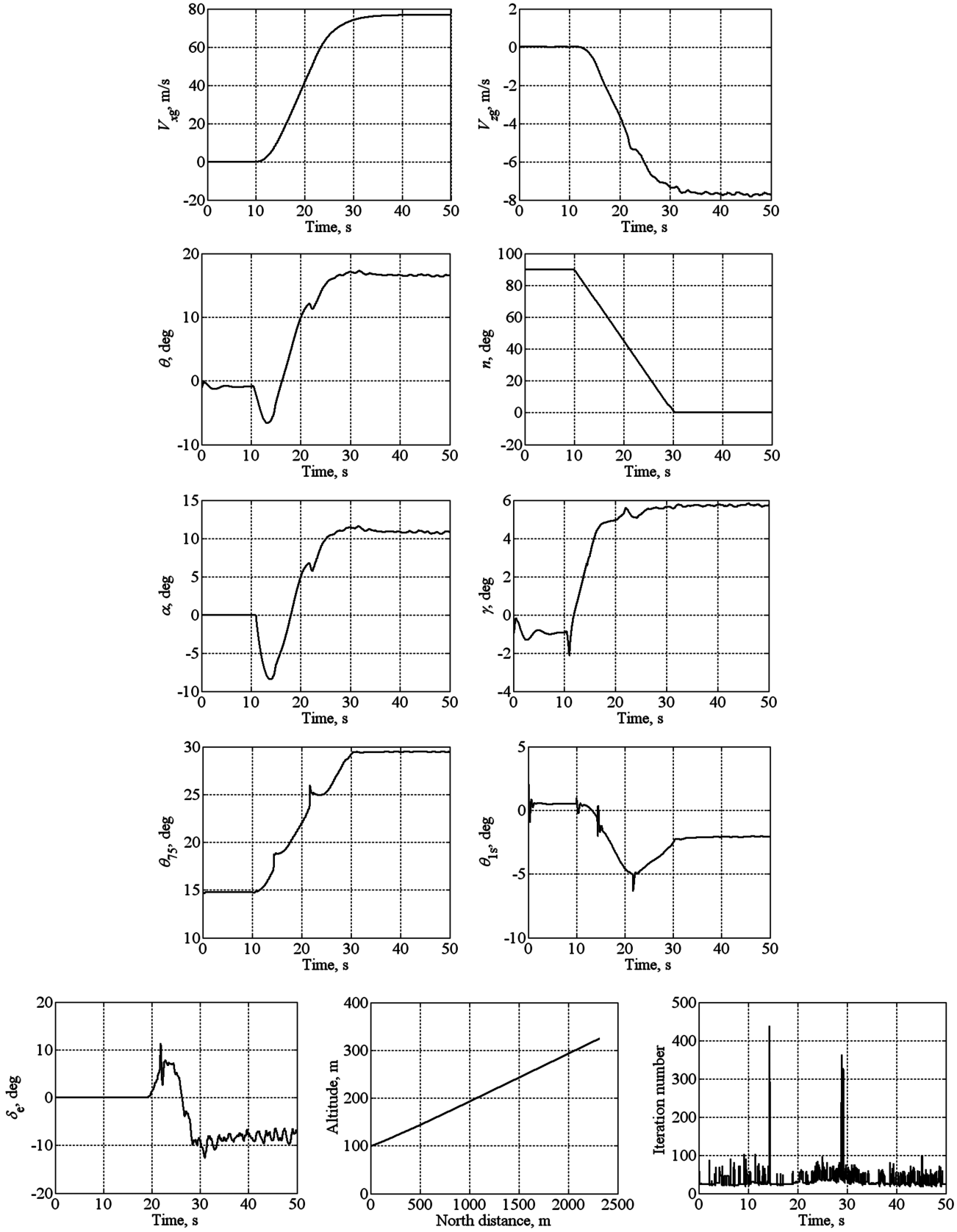

Fig. 14 Simulation results for tilt rotor transitioning and climbing from hover.

Figs. 12, 14, and 15, the iteration number has an average value of about 50. In Fig. 13, when the nacelle angle cannot tilt with the maximal angular velocity, the iteration number is larger and the performance degrades. Therefore, allowing the nacelle angle to tilt with the maximal angular velocity will be beneficial to the performance of the algorithm.

V. Conclusions

Two different approaches were required to achieve the autonomous transition control of two types of V/STOL aircraft. The two types of V/STOL aircraft considered were a fixed-wing vectored-thrust aircraft and a tilt rotor aircraft. The dynamic

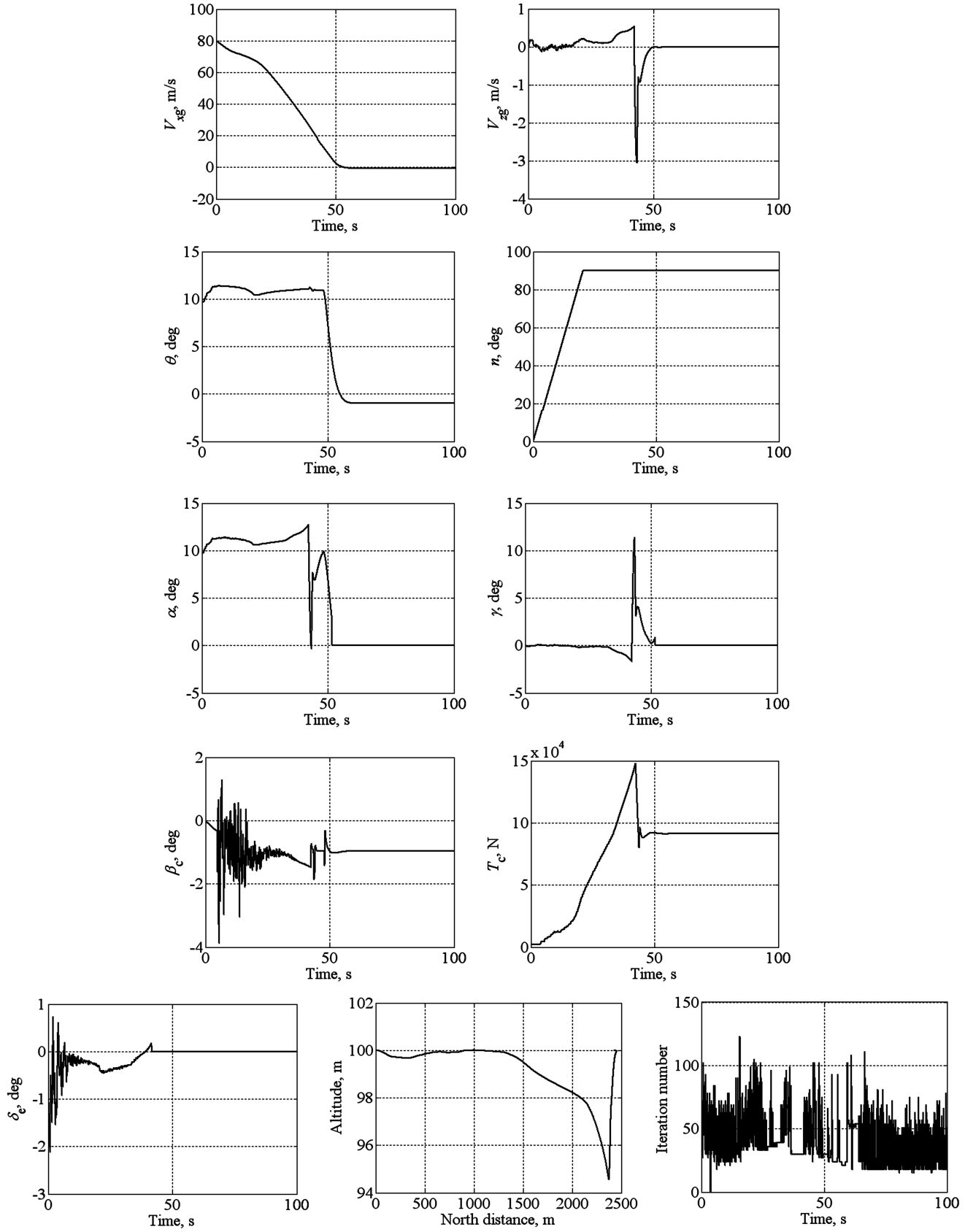

Fig. 15 Simulation results for tilt rotor transitioning from fixed-wing mode to helicopter mode hover.

models of the aircraft were nonlinear, nonaffine in the control inputs, nonanalytic, and multi-input, with some control inputs having end value constraints that were consistent with the goal of transitioning from hover to forward flight. It was not possible to use the same method to control both types of aircraft, because at low dynamic pressure the control effector arrangement on the tilt rotor aircraft makes it impossible to rapidly increase the pitch angle while simultaneously increasing velocity. Longitudinal dynamic simulation results show that the application of each method to the aircraft type for which it has been designed can

successfully achieve the autonomous transition from hover to forward flight.

Acknowledgments

This work is supported by the Tsinghua University Basic Research Foundation Grant JC2003029 and the China Postdoctoral Science Foundation Grant 20060390468. The authors would like to thank all of the members of the Intelligent Flight Control Group, State Key Lab of Intelligent Technology and Systems, Department of Computer Science and Technology, Tsinghua University.

References

[1] Ransone, R., "An Overview of Experimental VSTOL Aircraft and Their Contributions," AIAA Paper 02-5979, Nov. 2002.

[2] Stevens, B. L., and Lewis, F. L., "Aircraft Dynamics and Classical Control Design," *Aircraft Control and Simulation*, 2nd ed., Wiley, Hoboken, NJ, 2003, pp. 254–381.

[3] Snell, S. A., Enns, D. F., and Garrard, W. L., "Nonlinear Inversion Flight Control for a Supermaneuverable Aircraft," *Journal of Guidance, Control, and Dynamics*, Vol. 15, No. 4, 1992, pp. 976–984.

[4] Enns, D., Bugajski, D., Hendrick, R., and Stein, G., "Dynamic Inversion: An Evolving Methodology for Flight Control Design," *International Journal of Control*, Vol. 59, No. 1, 1994, pp. 71–91. doi:10.1080/00207179408923070

[5] Kim, B. S., and Calise, A. J., "Nonlinear Flight Control Using Neural Networks," *Journal of Guidance, Control, and Dynamics*, Vol. 20, No. 1, 1997, pp. 26–33.

[6] Doman, D. B., and Ngo, A. D., "Dynamic Inversion-Based Adaptive/ Reconfigurable Control of the X-33 on Ascent," *Journal of Guidance, Control, and Dynamics*, Vol. 25, No. 2, 2002, pp. 275–284.

[7] Poonamallee, V. L., Doman, D. B., Yurkovich, S., Oppenheimer, M. W., and Serrani, A., "A Nonlinear Programming Approach for Control Allocation," *Proceedings of the 2004 American Control Conference*, Inst. of Electrical and Electronics Engineers, New York, 2004, pp. 1689–1694.

[8] Bolender, M. A., and Doman, D. B., "Nonlinear Control Allocation Using Piecewise Linear Functions," *Journal of Guidance, Control, and Dynamics*, Vol. 27, No. 6, 2004, pp. 1017–1027.

[9] Luo, Y., Doman, D. B., Serrani, A., Oppenheimer, M. W., and Yurkovich, S., "Model Predictive Dynamic Control Allocation with Actuator Dynamics," *Proceedings of the 2004 American Control Conference*, Inst. of Electrical and Electronics Engineers, New York, 2004, pp. 1695–1700.

[10] Petersen, J., and Bodson, M., "Constrained Quadratic Programming Technique for Control Allocation," *Proceedings of the 42nd IEEE Conference on Decision and Control*, Inst. of Electrical and Electronics Engineers, New York, 2003, pp. 3378–3383.

[11] Bodson, M., "Evaluation of Optimization Methods for Control Allocation," *Journal of Guidance, Control, and Dynamics*, Vol. 25, No. 4, 2002, pp. 703–711.

[12] Schierman, J. D., Ward, D. G., Hull, J. R., Gandhi, N., Oppenheimer, M. W., and Doman, D. B., "Integrated Adaptive Guidance and Control for Re-Entry Vehicles with Flight-Test Results," *Journal of Guidance, Control, and Dynamics*, Vol. 27, No. 6, 2004, pp. 975–988.

[13] Kannan, S. K., and Johnson, E. N., "Adaptive Trajectory Based Control for Autonomous Helicopters," *Digital Avionics Systems Conference*, Vol. 2, Inst. of Electrical and Electronics Engineers, New York, 2002, pp. 8D1-1-12.

[14] Calise, A. J., and Rysdyk, R. T., "Adaptive Model Inversion Flight Control for Tiltrotor Aircraft," AIAA Paper 97-3758, Oct. 1997.

[15] Rysdyk, R. T., and Calise, A. J., "Adaptive Nonlinear Control For Tiltrotor Aircraft," *Proceedings of the IEEE International Conference on Control Applications*, 1998, pp. 980–984.

[16] Mehra, R. K., Prasanth, R. K., and Gopalaswamy, S., "XV-15 Tiltrotor Flight Control System Design Using Model Predictive Control," *Proceedings of the IEEE Aerospace Conference, Aspen, Colorado*, Vol. 2, Inst. of Electrical and Electronics Engineers, New York, 1998, pp. 139–148.

[17] Mehra, R. K., Prasanth, R. K., Bennett, R. L., Neckels, D., and Wasikowski, M., "Model Predictive Control Design for XV-15 Tilt Rotor Flight Control," AIAA Paper 01-4331, Aug. 2001.

[18] Yang, X. L., Zhu, J. H., Huang, X. L., Hu, C. H., and Sun, Z. Q., "Modeling and Simulation for Tiltrotor Airplane," *Acta Aeronautica et Astronautica Sinica*, Vol. 27, No. 4, 2006, pp. 584–587.

[19] Walker, G. P., and Allen, D. A., "X-35B STOVL Flight Control Law Design and Flying Qualities," AIAA Paper 02-6018, Nov. 2002.

[20] Georgie, J., and Valasek, J., "Evaluation of Longitudinal Desired Dynamics for Dynamic-Inversion Controlled Generic Reentry Vehicles," *Journal of Guidance, Control, and Dynamics*, Vol. 26, No. 5, 2003, pp. 811–819.

[21] Papageorgiou, G., and Glover, K., "Robustness Analysis of Nonlinear Flight Controllers," *Journal of Guidance, Control, and Dynamics*, Vol. 28, No. 4, 2005, pp. 639–648.

[22] Nocedal, J., and Wright, S. J., "*Quasi-Newton Methods*," *Numerical Optimization*, Springer–Verlag, New York, 1999, pp. 194–201.